

M. D. Barringer
K. A. Thole

Department of Mechanical and Nuclear
Engineering,
Pennsylvania State University,
University Park, PA 16802

M. D. Polanka
J. P. Clark
P. J. Koch

Turbines Branch,
Turbine Engine Division,
Air Force Research Laboratory,
WPAFB, OH 45433

Migration of Combustor Exit Profiles Through High Pressure Turbine Vanes

The high pressure turbine stage within gas turbine engines is exposed to combustor exit flows that are nonuniform in both stagnation pressure and temperature. These highly turbulent flows typically enter the first stage vanes with significant spatial gradients near the inner and outer diameter endwalls. These gradients can result in secondary flow development within the vane passage that is different than what classical secondary flow models predict. The heat transfer between the working fluid and the turbine vane surface and endwalls is directly related to the secondary flows. The goal of the current study was to examine the migration of different inlet radial temperature and pressure profiles through the high turbine vane of a modern turbine engine. The tests were performed using an inlet profile generator located in the Turbine Research Facility at the Air Force Research Laboratory. Comparisons of area-averaged radial exit profiles are reported as well as profiles at three vane pitch locations to document the circumferential variation in the profiles. The results show that the shape of the total pressure profile near the endwalls at the inlet of the vane can alter the redistribution of stagnation enthalpy through the airfoil passage significantly. Total pressure loss and exit flow angle variations are also examined for the different inlet profiles. [DOI: 10.1115/1.2950076]

Introduction

The performance of gas turbine engines is highly dependent on the operation and durability of the hot section, which includes the combustor and high pressure turbine. The vanes and blades of the high pressure turbine must operate in a very harsh flow environment that includes elevated turbulence and significant spatial gradients of pressure and temperature. The flow and thermal field gradients are most prevalent at the turbine inlet along the inner diameter (ID) and outer diameter (OD) endwalls. Their shape and complexity originate from intense flow interactions that take place within the upstream combustor section. The spatial variations in pressure and temperature at the turbine inlet result in nonuniform heat transfer to the vanes and blades that can damage the components. The high turbulence typically found at the exit of an aeroengine combustor acts to intensify this heat transfer by increasing local convection heat transfer coefficients.

The mean radial flow and thermal profiles that enter the high pressure turbine can have gradients near the ID and OD endwalls that are either positive or negative. This means that the local total pressure or total temperature near the endwalls can be larger or smaller than that near midspan. Typically, turbine durability engineers prepare for the worst case when designing the high pressure vanes and blades without knowing specifically how the combustor exit profiles are redistributed from vane inlet to blade inlet. For example, designers often use a radial pressure profile consistent with a flat plate turbulent boundary layer as the inlet condition to the turbine and assume a temperature drop across the vane due to cooling for a given combustor exit temperature variation. A turbulent boundary layer is characterized by decreasing total pressure with increasing proximity to the endwall. However, more realistic combustor exit flows can result in turbine inlet profiles that are significantly different than that. For example, some turbines experience inlet conditions where there is an increase in total pressure

near the endwall that is caused by a combination of combustor liner film cooling and a contraction at the combustion chamber exit. Additionally, the one dimensional analyses often used to assess temperature redistribution are known to be lacking. So, what is needed are accurate experimental studies with realistic vane inlet profiles and modern turbine geometries coupled with Reynolds-averaged Navier-Stokes (RANS)-based numerical analyses.

Relevant Past Studies

Computational and experimental studies have been performed that have investigated certain effects of turbine inlet profiles. One of the earliest studies was performed by Munk and Prim [1] in 1947 who showed mathematically that streamline patterns would remain unchanged in a vane passage with respect to variations in inlet total enthalpy provided the inlet total pressure field was constant. This finding is applicable to a hot streak propagating through a vane passage. The presence of the hot streak does not affect the pressure field in the vane passage provided the inlet total pressure field remains unchanged. Langston [2] showed in 1980 that a flat plate turbulent boundary layer at the inlet of a turbine vane separates near the endwall and forms a horseshoe vortex. The part of the vortex proceeding to the pressure side of the vane develops into a passage vortex, and the portion that proceeds to the suction side of the vane develops into a relatively smaller and weaker counter-rotating vortex. This counter-rotating vortex is sometimes referred to as a corner vortex since it is restricted to the endwall junction region along the vane suction side. These secondary flow vortices have a direct impact on the migration of the primary flow by circulating it toward or away from the endwalls and vane surfaces.

Studies by Hermanson and Thole [3] have shown that the total pressure field is the driving force in the development of secondary flows and heat transfer present in turbine vane passages. Colban et al. [4] studied the effects of varying film cooling flow through the liner and exit junction slot of a large-scale, low speed combustor simulator on the adiabatic effectiveness and secondary flow development within a downstream turbine cascade. Their study documented the vane passage secondary flow vectors for different vane

Contributed by the International Gas Turbine Institute of ASME for publication in the JOURNAL OF TURBOMACHINERY. Manuscript received July 26, 2007; final manuscript received January 3, 2008; published online January 23, 2009. Review conducted by David Wisler. Paper presented at the ASME Turbo Expo 2007: Land, Sea and Air (GT2007), Montreal, QC, Canada, May 14–17, 2007.

inlet total pressure profiles and reported a counter-rotating vortex located above the passage vortex for a vane inlet pressure profile containing an inflection point near the endwall.

Computational studies performed by Boyle and Giel [5] and Dorney and Schwab [6] as well as experimental studies performed by Cattafesta [7], Shang et al. [8], Chana et al. [9], and Povey et al. [10] have all showed that heat transfer to turbine vanes and blades is affected by the presence of a nonuniform inlet temperature profile. The heat load to the vane and endwall regions is typically reduced when a nonuniform temperature profile consistent with a combustor exit is present at the inlet of the turbine stage, relative to a uniform turbine inlet temperature profile. The heat load to the rotor blades, however, typically increases especially along the pressure side. This result was first determined from studies performed by Butler et al. [11] and later verified by Slexer and Giles [12].

The current literature to date suggests that certain heat transfer trends within the turbine section are due to nonuniform inlet temperature and pressure conditions. Studies including Barringer et al. [13], Shang et al. [8], Chana et al. [9], Butler et al. [11], and Slexer and Giles [12] have reported significant augmentation of heat transfer along the suction side of the vanes and the pressure side of the blades in both the hub and tip regions using nonuniform inlet temperature profiles. The literature, however, contains little experimental data that documents the effects of realistic total pressure profiles at the turbine inlet.

An improved understanding of how these realistic turbine inlet profiles affect the flow development and heat transfer within the turbine is needed. This can, in part, be accomplished by studying how different radial profiles of total pressure and temperature are redistributed as the flow passes through the high pressure vane passages. The goal of the current study is to examine the migration of different turbine inlet profiles by analyzing both the vane inlet and corresponding exit profile shapes. The results from this study will aid turbine designers by providing them with an improved picture of what blade inlet profiles they should anticipate for certain combustor exit profile shapes.

Experimental Facility

The experimental facility used in this study is the Turbine Research Facility (TRF) located within the Air Force Research Laboratory (AFRL) at Wright Patterson Air Force Base. This facility operates in a short duration blowdown manner in which several aerothermal engine parameters are matched. These nondimensional parameters include Reynolds number, Mach number, pressure ratio, gas to metal temperature ratio, and corrected mass flow. The facility consists primarily of a large supply tank, a turbine test section, and two large vacuum tanks. The facility is described in more details in Haldeman et al. [14]; however, a brief summary of its operation is provided here.

The working fluid (nitrogen gas) is pressurized and heated within the supply tank prior to testing while at the same time the turbine section and vacuum tanks are evacuated. Testing then begins by activating the supply tank main valve, at which time the gas flows through the turbine test section and into the vacuum tanks. The mass flow rate of the working fluid is set by a variable area isolation valve located downstream of the main test section, which controls the turbine pressure ratio. The duration of the tests in the current study was approximately 5 s, which was dependent on the size of the turbine being tested. Due to the short test duration, all measurements were recorded simultaneously in real time. The data were simultaneously acquired across multiple 12 bit channels having a maximum frequency response of 100 kHz and multiple 16 bit channels having a maximum frequency response of 200 kHz. Signal conditioning on each channel was performed using low pass filters and built-in amplifiers. All data processing was performed at a later time.

The turbine test section is a true scale, fully annular, single turbine stage consisting of vanes and blades. The tests in the cur-

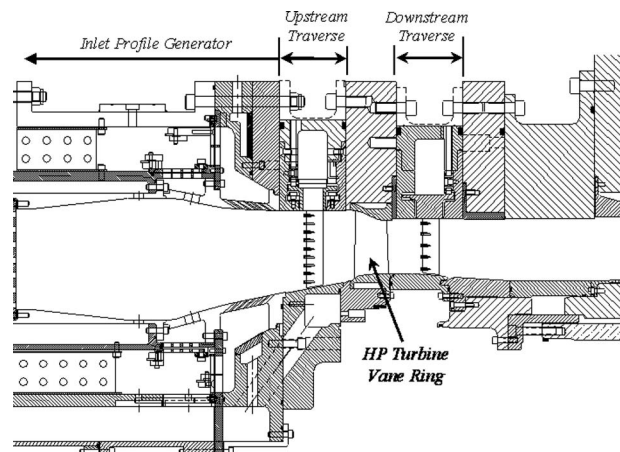


Fig. 1 Drawing of the TRF test rig in a vane-only configuration with the inlet profile generator

rent study were performed using a vane only configuration, as shown in the facility drawing in Fig. 1. The turbine inlet profile generator, documented in Barringer et al. [15], was used in the current study to allow turbine testing with inlet profiles of pressure and temperature representative of those exiting engine combustors as well as realistic turbulence intensities and length scales. The inlet profile generator can also be seen in Fig. 1 upstream of the test vane ring. The generator operates by mimicking an aeroengine combustor in which it injects several different flow streams at different temperatures into a central chamber via dilution holes and film cooling holes. The injection flow rates, momentum flux ratios, and temperatures of the different flow streams are varied depending on the desired turbine inlet profile shapes.

The turbine inlet and exit profiles are measured using multiple instrumentation rakes located on traverse rings upstream and downstream of the turbine section. The rakes, shown in Fig. 2, contain multiple thermocouples or pressure transducers that are spaced to obtain measurements over equal annular flow areas. The tests discussed in this study involved traversing these rakes by approximately 90 deg during the blowdown to obtain both radial and circumferential data. For the turbine inlet profiles being analyzed in the current study, a temperature rake was used containing seven 0.0254 mm diameter thermocouple beads with a thermal time constant of approximately 1.1 ms. Two pressure rakes were also used each containing nine miniature high frequency pressure transducers. All flow and thermal measurements were sampled at 20 kHz.

The pressure transducers were calibrated in situ prior to each test using a Ruska standard. A typical calibration uncertainty for

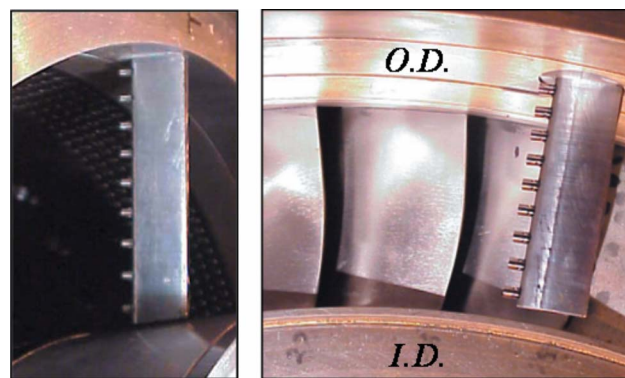


Fig. 2 Instrumentation rakes mounted in the upstream (left) and downstream (right) traverses

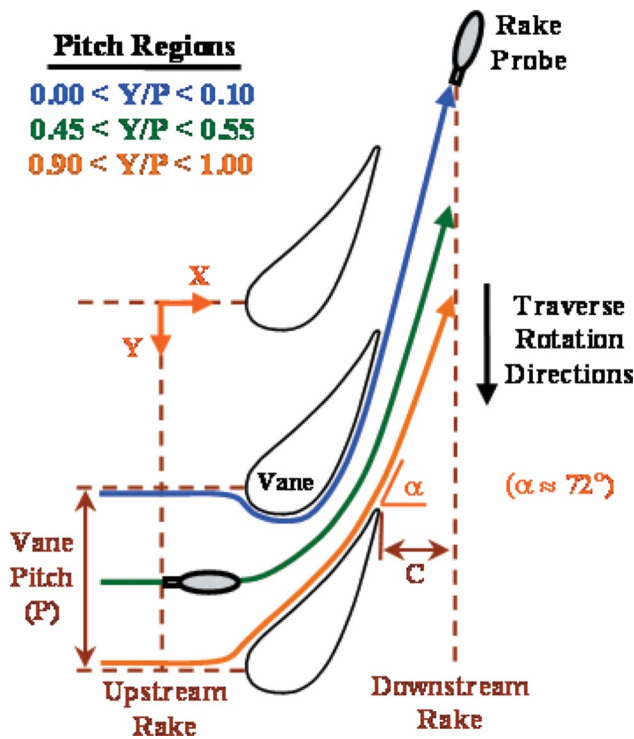


Fig. 3 Schematic showing the three different flow path regions and measurement locations

the transducers was less than 0.05% of full scale. The overall uncertainty for these transducers was raised 0.40% due to the short term drift known to exist between time of calibration and time of the run. The thermocouple wire used to manufacture the beads was calibrated in a Kaye temperature bath against a platinum RTD standard accurate to 0.01 K. The 0.0254 mm beads in the rakes were calibrated to an accuracy of 1.5 K.

Test Conditions and Measurements

The pressure and temperature profiles that are analyzed in this study were generated during a series of tests whose flow conditions are reported in more details in Barringer et al. [15]. To summarize, the mean flow conditions at the turbine inlet for all of the profiles presented in this study correspond to a mean Reynolds number of $Re=2.1\times 10^5$ and a mean axial Mach number of $M=0.1$. The turbulence intensity associated with these turbine inlet profiles was also documented during testing and was found to be in an elevated range between $Tu=20\text{--}30\%$. For a baseline test case with nearly uniform inlet pressure and temperature, the turbulence intensity was determined to be approximately 21% and the longitudinal integral length scale was approximately 30% of the vane pitch or 2.3 times the vane leading edge diameter.

To study the migration of the flow in both the radial and circumferential directions as it passes through the vane passage, three pitch regions are considered. The schematic shown in Fig. 3 highlights the locations of the three different flow pitch regions. The uppermost streamline is centered at $Y/P=0.05$ and is indicative of the flow conditions present near the suction side of the vane between $0.00 < Y/P < 0.10$. The flow path region in the middle is centered at $Y/P=0.50$ and is representative of the flow conditions that are present near the midpassage between $0.45 < Y/P < 0.55$. The lowermost streamline is centered at $Y/P=0.95$ and is indicative of the flow conditions that are present near the pressure side of the vane between $0.90 < Y/P < 1.00$.

The vanes have a nominal exit flow angle of $\alpha=72$ deg and the downstream traverse rakes are aligned according to this same angle. The axial distances from the trailing edge of the vanes to

the downstream rake measurement location and from the leading edge to the upstream rake measurement location are both approximately equal to one vane axial chord length. During rotation, the traverses move from the suction side of the vane toward the pressure side.

Computational Techniques

In an effort to supplement the experimental data obtained in this study, the flow through the turbine vane was analyzed via the 3D time-accurate RANS solver of Dorney and Davis [16]. The flow solver is itself a further development of the Rai code [17,18]. The solver is second order accurate in time and third order accurate in space, and numerical closure is obtained via a modified version of the Baldwin-Lomax algebraic turbulence model [16].

In a previous study, Prahl et al. [19] demonstrated the grid counts as well as the viscous and cooling model details necessary to predict the redistribution of stagnation quantities in turning ducts as well as modern high pressure turbine stages. The results of that previous study were used as a guide for the simulations performed here both in terms of grid-count and turbulence-model selection. Accordingly, an O-H grid was employed with counts for the O-grid of $161 \times 40 \times 49$ in the axial, circumferential, and radial directions, respectively. For the H-grid, the grid counts were $100 \times 41 \times 49$. The near-wall grid spacing was set at $0.25 \mu\text{m}$ to minimize the local grid Reynolds number based on wall units, which was everywhere less than unity. As regards to the viscous model employed here, Prahl et al. [19] noted that the redistribution of 1D profiles was adequately captured with an algebraic turbulence model as it was with more computationally expensive two equation turbulence models. So, the use of the Baldwin-Lomax turbulence model [16] is justified given the goals of the current study.

A pair of simulations was performed, and experimentally determined boundary conditions consistent with Profiles B and D (to be discussed in the next section) were used to obtain flow solutions. These profiles were selected for code validation because they represented the extreme variation of the profiles tested in the experiment. The experimental data used for boundary conditions included the inlet total pressure and temperature, the inlet flow angle, and the vane exit static pressure. Additionally, an isothermal wall thermal boundary condition was employed, and the wall temperature was set at a level consistent with time-averaged measurements made with thin-film heat flux gauges on the vane and endwall surfaces. Results of the simulations were postprocessed in a manner consistent with the experimental measurements via tools available in the AFRL Turbine Design and Analysis System, which has been previously described [20,21].

Turbine Vane Inlet Flow

Four radial profiles of total pressure measured at the turbine vane inlet are shown in Fig. 4. Each profile that is shown represents the mean conditions across three vane pitches. The pitchwise uniformity of the four inlet total pressure profiles in the circumferential direction was found to be excellent from vane to vane. This uniformity revealed that the radial profiles measured upstream of the vane were nearly the same for each of the three pitch regions. This is important in making comparisons of the exit profiles because it ensures that the same inlet conditions are present for each pitch. The total pressure has been normalized by use of the total pressure coefficient C_p , which references the local total pressure to the midspan total pressure and divides the result by the mean dynamic pressure of the flow entering the vane passage. A positive value of C_p indicates that the local total pressure is larger than that measured at the midspan, and a negative value of C_p indicates that the local total pressure is smaller than that measured at the midspan. This pressure normalization is helpful in illustrating the important gradients that are typically found in turbine inlet pressure profiles near the endwalls.

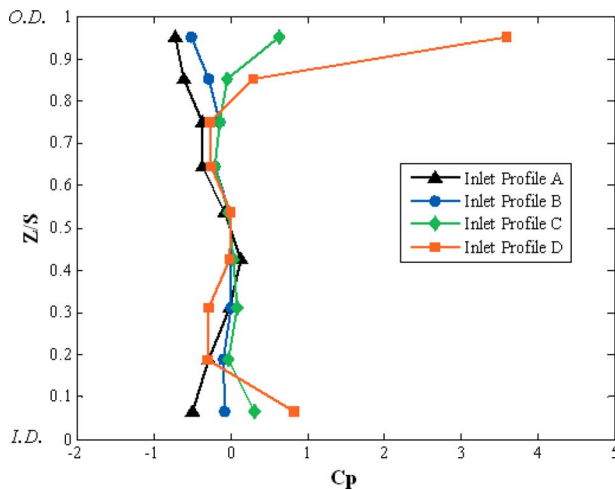


Fig. 4 Radial profiles of total pressure at the vane inlet

The first total pressure profile in Fig. 4 to be considered is Inlet Profile A, which is characterized by a parabolic shape with a maximum total pressure at $Z/S=0.43$ near midspan and lower total pressures near both the ID and OD endwalls. Inlet Profile A is characteristic of flow having a turbulent boundary layer profile on both the ID and OD endwalls. Inlet Profile B is characterized by near uniform total pressure over the majority of the vane span with slightly lower total pressure near the OD endwall. Inlet Profile C possesses near uniform total pressure over the majority of the vane span but has higher total pressure near both the ID and OD endwalls. Inlet Profile D is also characterized by near uniform total pressure over the majority of the vane span but has much higher total pressure near the ID and OD endwalls.

This set of four inlet pressure profiles was considered important for the current investigation, since it included both lower and higher total pressure scenarios near both endwalls relative to midspan. The difference in total pressure near the endwalls was the result of varying amounts of film cooling that entered the turbine along the endwalls. The near uniform pressure that is present near the midspan region is the result of intense dilution mixing that is present upstream and typically found in combustor exit flows.

The corresponding total temperature profiles measured upstream of the vanes are shown in Fig. 5. These radial profiles are also spatial averages of the temperature conditions in the circumferential direction across the inlet of three vane pitches. The total

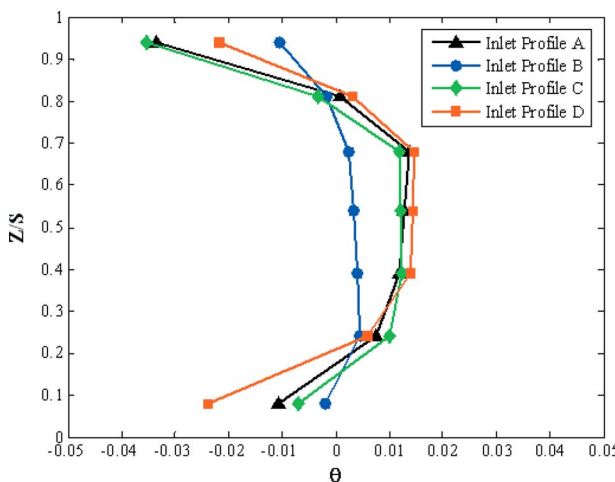


Fig. 5 Radial inlet profiles of total temperature corresponding to the pressure profiles in Fig. 4

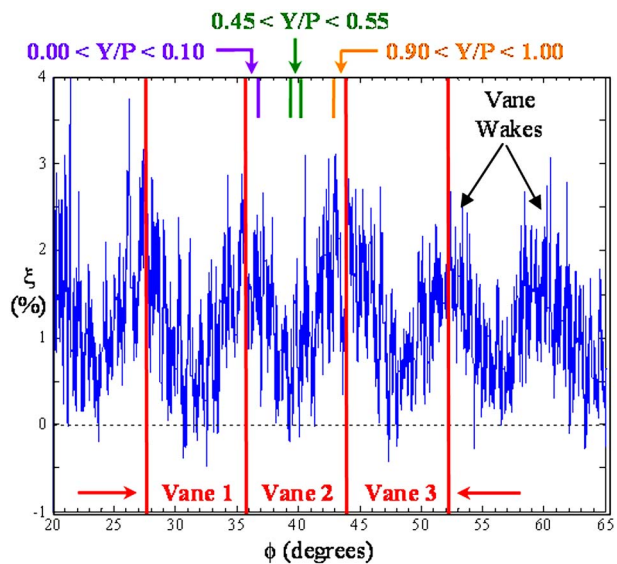


Fig. 6 Total pressure loss across the vanes at $Z/S=0.19$ for Inlet Profile B

temperature has been normalized by the use of a temperature coefficient θ , which references the local total temperature to the average temperature measured upstream of the vanes. These spanwise thermal profiles were also found to be near uniform in the pitch direction. The thermal Inlet Profiles A and C are almost identical with warmer fluid near midspan and cooler fluid near the endwalls. The thermal Inlet Profile B is more uniform across the span, and the thermal Inlet Profile D is a near symmetric profile about midspan with warmer fluid near midspan and cooler fluid near the endwalls.

Turbine Vane Exit Flow

The relative position of the upstream and downstream traverse rakes with respect to the vanes was verified by comparing their rotational timing to the wake profiles measured downstream of the vanes. Figure 6 shows an example of a wake profile measured downstream of multiple vanes for Inlet Profile B (near uniform inlet conditions) at a span location of $Z/S=0.19$. The total pressure loss, defined in the Nomenclature, is plotted versus traverse rotation angle for several vane pitches.

A low value of loss (ξ) implies that the total pressure measured downstream of the vane is nearly the same as the total pressure measured upstream at the vane inlet. A low value of loss, therefore, takes place near midpitch ($Y/P=0.50$) in which the flow experiences a little pressure drop as it passes through the vane passage. A higher loss corresponds to a lower total pressure relative to that measured upstream of the vane at the same pitch location. Higher values of loss exist in pitch regions in the vicinity of the vane airfoil trailing edge, for example, near the vane suction side ($Y/P=0.05$) or near the vane pressure side ($Y/P=0.95$). The three flow path pitch regions are also indicated near the top of Fig. 6 for one of the vane passages to illustrate how the vane wake profile shape corresponds to each region. The total pressure loss across the vanes at this span location ($Z/S=0.19$) was found to be within $0 < \xi < 3\%$ with a mean value of $\bar{\xi} = 1.25\%$.

The total pressure loss across the vanes was also investigated for Inlet Profile B as a function of vane span location for multiple vane pitches, as shown in Fig. 7. Figure 7(a) indicates that the wake profile shape is more evident near the ID compared to the midspan region and near the OD. This result was also found for each of the four inlet pressure profiles studied. This is explained

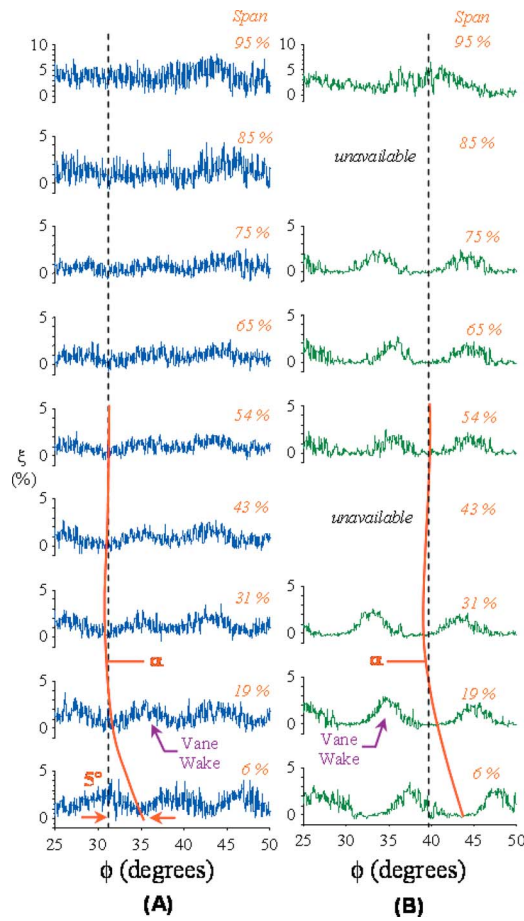


Fig. 7 Total pressure loss ξ (%) across the vane for Inlet Profile B with high freestream turbulence 21% (a) and low freestream turbulence 1% (b), shown for three vane pitches

by the fact that the vane exit velocities near the ID are higher than at the midspan and OD. These higher exit velocities were verified by both measurements of the vane exit static pressure and the results of RANS simulations. The higher exit velocities near the ID are a consequence of radial equilibrium considerations at the exit. Therefore, the wake profile should be more noticeable near the ID.

It can also be seen in Fig. 7(a) that the wake profile at $Z/S=0.06$ is nearly 180 deg out of phase with the wakes near midspan. This phase shift can be verified by examining the alignment of the wake peaks and valleys at 6% span versus 19% span. It was determined that this phase shift in wake profile was due to a change in the vane exit flow angle α of approximately $\Delta\alpha=5.0$ deg between midspan and the ID endwall. The solid line in Fig. 7(a) is an estimate of the radial profile shape of the exit flow angle from the ID endwall to the OD endwall.

Figure 7(b) is a comparison of the total pressure loss across the same vane ring when testing with uniform inlet conditions but with low freestream turbulence near 1%. This low freestream turbulence data was taken during a study by Urbassik et al. [22], and when it is compared to the data in Fig. 7(a) from the current study, it can be seen that the high freestream turbulence is resulting in less total pressure being recovered downstream of the vanes. This is evident by first examining the region of the data traces near $\xi=0\%$ at each span location. For the low freestream turbulence case, the data traces exhibit zero loss over a larger range of circumferential traverse rotation than the high freestream turbulence case. Second, integrating the total pressure loss over both the vane pitch and radius yields an overall mean loss of $\bar{\xi}=1.20\%$ for the

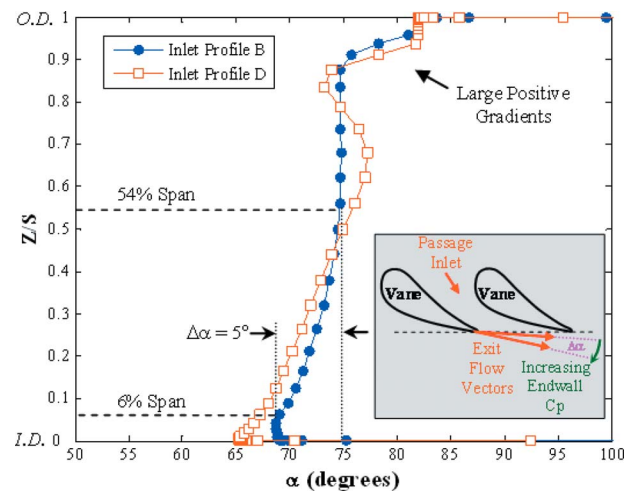


Fig. 8 CFD prediction of the exit flow angle as a function of vane span

high turbulence case (Inlet Profile B) and $\bar{\xi}=0.81\%$ for the low turbulence case. The higher turbulence is resulting in the exit flow loss profiles being more mixed out. In addition, when comparing Fig. 7(a) to Fig. 7(b), it can be seen that the rms of the loss traces is much less for the lower turbulence case. This is consistent with the lower level of random unsteadiness expected in the low turbulence case.

All of these results are consistent with the findings by Ames et al. [23] who reported that high freestream turbulence acted to enhance the mixing downstream of a turbine vane as well as broaden the wakes and increase the losses. They also reported that as the flow developed from $\frac{1}{4}$ to $\frac{1}{2}$ axial chord downstream of the vane, the wakes spread and decreased in amplitude and that this spreading was more pronounced at a high freestream turbulence condition ($\sim 15\%$) relative to a low freestream turbulence condition ($\sim 1\%$).

It is also evident from Fig. 7(a) that the total pressure loss in the vicinity of the OD endwall at 95% span is much higher than the loss measured at all other span locations. Note the scale used at this span location ($Z/S=0.95$) is $0 < \xi < 10\%$ loss, while the scale used at all other span locations was $0 < \xi < 5\%$ loss. This difference in plot was included to fully display the larger loss measured at $Z/S=0.95$ while also ensuring that the wakes at the other span locations were identifiable. It was determined that the large pressure loss near the OD corresponded to the same span region in which a sharp change in the vane exit flow angle was predicted. Since the loss profiles are mixed out circumferentially from midspan to the OD, the shift in exit flow angle is not clearly evident from the wake profiles in Fig. 7(a). However, a prediction of the exit flow angle as a function of span location for Inlet Profile B is presented in Fig. 8. The prediction of the overall shift in exit flow angle between $0.06 < Z/S < 0.54$ for Inlet Profile B is approximately $\Delta\alpha=5$ deg, which compares well with the data in Fig. 7(a). In the span region $0.50 < Z/S < 0.85$, α is predicted to be uniform near $\alpha=74$ deg, which is also consistent with the data. At span locations above $Z/S > 0.85$, a large positive gradient is present, which is believed to correspond to the large pressure loss measured near the OD.

A comparison is also made in Fig. 8 between the exit flow angles for Inlet Profiles B and D, which have very different pressure profile shapes. Inlet Profile B has near uniform total pressure across the span and Inlet Profile D has uniform total pressure near midspan but has much higher total pressure near both the ID and OD endwalls. Figure 8 shows that the exit flow angle experienced for Inlet Profile D near the ID endwall is several degrees lower than that corresponding to Inlet Profile B. This reduction in exit

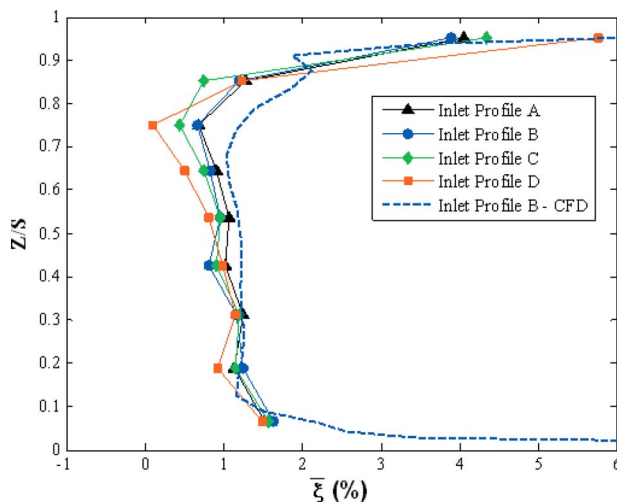


Fig. 9 Average total pressure loss as a function of span location for the different inlet profiles

flow angle is physically explained in the schematic shown in Fig. 8. As the total pressure is increased at the vane passage inlet near the ID endwall, the momentum of the fluid entering the passage also increases. At these higher inlet pressures, the momentum of the fluid becomes large enough to overcome the cross passage pressure gradient from pressure side to suction side. This results in the flow not following the curvature of the suction side of the vane near the passage exit as closely as it would at lower inlet pressures (lower inlet momentum), thus reducing the exit flow angle. In addition, the relatively high pressure region near the passage exit along the pressure side increases as the passage inlet total pressure increases. This forces the flow leaving the passage along the vane pressure side to turn more in the axial direction into the relatively lower pressure region along the suction side.

Near the OD within the span region $0.85 < Z/S < 0.95$, both inlet profiles are predicted to have large positive gradients in the exit flow angle. This implies that the large total pressure loss experienced near the OD at the vane exit is not associated with the vane inlet flow conditions. The loss is more likely due to the vane and endwall geometry in this span region producing strong secondary flows. In general, this high pressure turbine vane results in an exit flow angle that increases with increasing span location due to the vane metal angle slightly increasing from hub to tip. The important result is that the different inlet pressure profiles result in different exit flow angle profiles by altering the fluids inlet momentum.

The average total pressure loss across the vanes at each measured span location is plotted in Fig. 9 for each inlet pressure profile. It can be seen that the loss is higher near the endwalls compared to midspan for each inlet profile. This is a result of the flow near the endwalls interacting with three wall surfaces (vane pressure side, vane suction side, and endwall) as compared to the midspan flow that interacts with only two wall surfaces (vane pressure side and vane suction side). The endwall acts to reduce the fluid momentum by increasing its aerodynamic drag. The presence of secondary flow vortices near the endwall and vane hub and tip surfaces also contributes to the higher loss experienced near the platforms.

The mean loss measured near the OD endwall at $Z/S=0.95$ is considerably higher than that measured near the ID endwall at $Z/S=0.06$ for each inlet profile. However, the simulation results, also shown in Fig. 9, for Inlet Profile B shows that the mean loss also becomes large at span locations close to the ID endwall. The agreement between the simulation and the data for Inlet Profile B

Table 1 Average total pressure loss near the OD as a function of the inlet total pressure coefficient

Inlet profile	C_p	$\bar{\xi}$ (%)
A	-0.72	4.05
B	-0.51	3.90
C	0.64	4.35
D	3.61	5.77

in Fig. 9 is relatively good, and it is believed that the measured data would also show an increase in near wall mean loss if data were taken at spans between $0 < Z/S < 0.06$.

The inlet profile shape does not significantly affect the mean loss values near the ID endwall at $Z/S=0.06$ but does affect the mean loss values near the OD endwall at $Z/S=0.95$. Table 1 shows that the mean loss measured near the OD endwall at $Z/S=0.95$ scales well with the value of the total pressure coefficient C_p measured at the vane inlet at the same span location. An increase in the inlet C_p coefficient value leads to an increase in the mean total pressure loss. It is believed that the loss at $Z/S=0.95$ is minimized when the inlet total pressure $C_p=0$. It is also believed that a similar relationship exists near the ID endwall below the span location $Z/S=0.06$, where it is believed that the effect between different inlet profiles becomes more pronounced.

Pressure Profile Migration

The redistribution of total pressure for Inlet Profile A as the flow passes through the vanes is shown in Fig. 10(a). The pressure profile measured downstream near midpitch has a similar shape to that of the inlet profile from $0.06 < Z/S < 0.75$; however, it possesses a large total pressure loss near the OD endwall. The two pressure profiles measured downstream near the suction and pressure sides of the vane are very similar in shape to one another and each have similar large total pressure losses near the OD endwall as does the midpitch profile. This implies that the flow is nearly uniform in the circumferential direction as it exits the vane near the OD but at a lower total pressure compared to the upstream OD. This pitchwise uniformity is consistent with the relatively weak wake formation shown near the OD in Fig. 7(a).

A similar negative total pressure gradient very close to the ID endwall within the span region $0.0 < Z/S < 0.06$ was observed in the results of the simulations (Fig. 9). The pitchwise uniformity near the OD was not found between $0.0 < Z/S < 0.55$. In this span region, rather, the midpitch exit profile shows relatively high pressure compared to the two exit profiles near the vane surfaces. This behavior is consistent with the stronger wake formation present near the ID in Fig. 7(a) and the gradual decrease in wake strength that is present with increasing span location.

The subsequent effect of changing the radial shape of Inlet Profile A by increasing the total pressure near both the ID and OD endwalls and how this influences the shape of the downstream pressure profiles are shown in Figs. 10(a)–10(d). As the upstream total pressure is increased along the endwalls, there is a general shift to the right toward increasing total pressure values for each of the downstream exit profiles. In addition, the three downstream profiles tend to become more uniform in the pitch direction over the majority of the vane span. For example, this is evident in the reduction of the wake strength near the ID at $Z/S=0.20$ when comparing the results for Inlet Profile A to the results for Inlet Profile D. It is clear from Fig. 10 that obtaining a relatively uniform exit pressure profile for this vane as an inlet condition to the downstream blade may not be possible, at least not without a very large total pressure near the endwalls at the combustor exit and vane inlet. This large total pressure at the inlet would be needed to overcome the large pressure loss experienced near the endwalls as the flow passes through the vane passage.

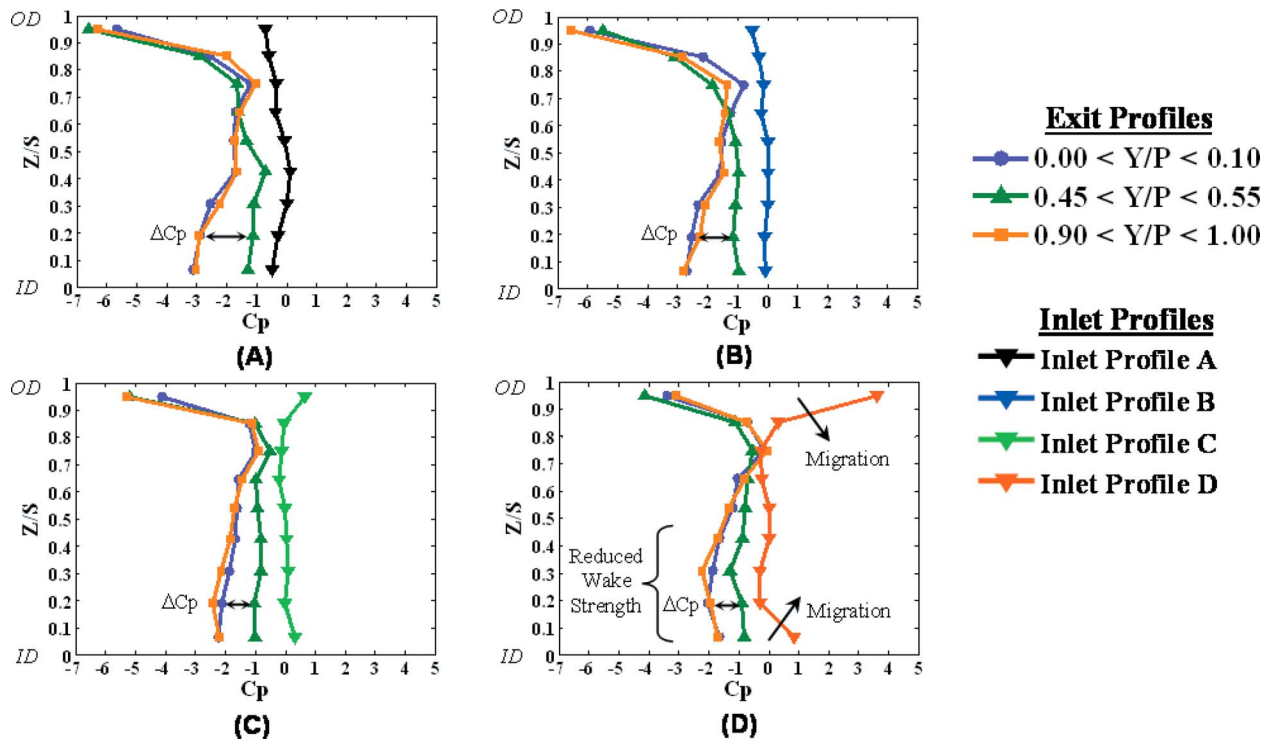


Fig. 10 Radial total pressure profiles measured at the vane exit for (a) Inlet profile A, (b) Inlet Profile B, (c) Inlet Profile C, and (d) Inlet Profile D

Another important finding was that Inlet Profiles C and D, which possess high total pressure near the endwalls at the inlet, result in fluid near the endwall migrating toward midspan, which is at a relatively lower total pressure. This migration is evident in comparing the exit profile C_p values and shapes in the span region $0.06 < Z/S < 0.30$ as well as near $Z/S = 0.75$ between Inlet Profiles A, B, C, and D. In the case of Inlet Profile D, this is resulting in total pressures at $Z/S = 0.75$ that are actually slightly higher for the exit profiles than for the vane inlet profile. Near the ID within the span region $0.0 < Z/S < 0.30$, in going from Inlet Profile A to Inlet Profile D, the total pressure gradients of the exit profiles have reversed direction from a decreasing C_p trend to an increasing C_p trend. In general, over the majority of the vane span, the pressure profiles at the vane exit within the pitch regions $0.0 < Y/P < 0.1$ and $0.9 < Y/P < 1.0$ are similar for each of the inlet pressure profiles, except near the OD. In the OD endwall region, the secondary flow losses are stronger along the vane pressure surface for Inlet Profiles A, B, and C. Figure 10(d) indicates that when the inlet total pressure near the OD endwall is very large, these secondary flow losses are similar along both vane surfaces (both pitch regions close to the vane surfaces).

The strength and size of these secondary flows near the endwalls are dependent on the inlet pressure profile shape near the endwall as well as the physical shape of the endwall and vane. Since the measurements were made one axial chord downstream of the vane passage exit, then the data are representative of vortex behavior (shape and size) near the passage exit. This means the vortices have already felt the influence of the endwall shapes and the vane turning, as well as the slight twist in vane metal angle. The larger the total pressure along the endwall (relative to midspan) at the vane inlet, the stronger these vortices become.

Temperature Profile Migration

The thermal migration of the inlet total temperature profiles as the flow passes through the vanes is now discussed using Fig. 11. The first temperature profile to be considered is that corresponding to Inlet Profile A, which is shown in Figure 11(a). This inlet

temperature profile has warmer fluid near midspan and cooler fluid near the endwalls. The three corresponding exit temperature profiles are nearly identical to one another across most of the span, which implies that almost uniform thermal conditions exist in the circumferential direction at the vane exit. It is believed that this pitchwise uniformity is the result of the elevated freestream turbulence and secondary flow mixing that occurs within the passage, which was also evident in the pressure and wake profiles discussed earlier. The similarity between the three exit profiles is an observation that is also present for Inlet Profiles B, C, and D shown in Fig. 11(b)–11(d). In addition, it is evident from Figs. 11(a)–11(d) that the mean flow temperature, T_{ave} , upstream at the vane inlet is larger than the mean flow temperature downstream at the vane exit. The difference between the two average flow temperatures is a measure of the total heat that is lost from the flow into the vane and endwall metal surfaces.

The three exit temperature profiles resulting from inlet Profile C are very similar to each other, and they are also similar to the exit temperature profile shapes for inlet Profile A. This is a result of Inlet Profiles A and C having similar temperature and pressure profile shapes over most of the vane span. The only noteworthy difference for Inlet Profile C takes place near the OD endwall where the reduction in flow temperature across the vane is larger for Inlet Profile C than for Inlet Profile A. This difference is attributed to Inlet Profile C having a positive C_p value of approximately $C_p = 1.0$ near the OD endwall, as compared to $C_p = -1.0$ for Inlet Profile A. The positive C_p value means that the turbine inlet pressure profile near the OD contains a forward facing pressure profile inflection point near the endwall. This results in a secondary flow structure that is different than for a typical turbulent boundary layer, in that it circulates flow toward both the endwall and midspan. As the flow passes through the turbine vane, this OD high pressure region directs colder fluid near the endwall toward the relatively lower total pressure midspan. This redistribution of colder fluid significantly reduces the fluid temperature from the OD endwall and into the midspan region.

A small increase in flow temperature is observed from the vane

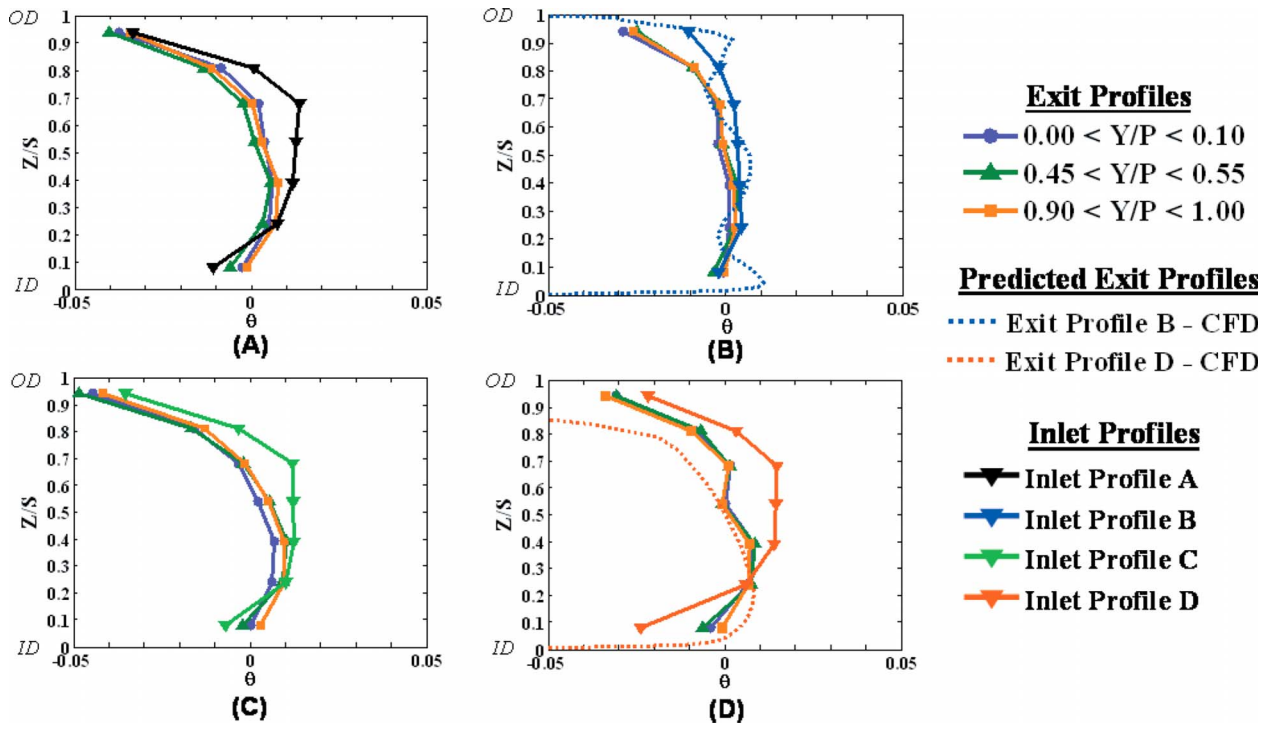


Fig. 11 Radial total temperature profiles measured at the vane exit for (a) Inlet Profile A, (B) Inlet Profile b, (c) Inlet Profile C, and (d) Inlet Profile D

inlet to the vane exit near the ID for each of the inlet profiles, with the exception of Inlet Profile B. Since Inlet Profile B has near uniform inlet pressure near the ID, the exit temperature profile near the ID should be similar to the inlet temperature profile, which is also near uniform, and the results in Fig. 11(b) verify that to be true. This result is consistent with the predictions of Munk and Prim [1]. Results of the simulations of the mean temperature profile at the vane exit plane for inlet Profiles B and D are also included in Fig. 11. In the simulation, a small increase in flow temperature is observed near the ID for inlet Profile B and a larger increase in flow temperature is seen for inlet Profile D. It is believed that the increase in flow temperature near the ID is caused by a migration of warmer fluid near midspan toward the ID endwall via secondary flow circulation within the vane passage.

Secondary flow vectors are plotted in Fig. 12 over contours of normalized exit temperature for the flow simulation with inlet Profiles B and D. The cutting plane was taken at an axial plane at 12% axial chord downstream of the vane trailing edge. The secondary flow vectors were calculated by subtracting the component of the local velocity parallel to the midspan, midpassage flow direction from the local flow vector [24]. Then, these secondary flow vectors were resolved into components on the cutting plane. These figures clearly show the wake regions. Within these wakes, the secondary flow vectors show a large movement of flow from the OD to the ID. The color contours indicate that this flow is carrying cold fluid from the OD wall down toward the ID. As shown in Figure 12(a), inlet Profile B results in far less thermal migration toward the ID than in inlet Profile D (Figure 12(b)). This is consistent with the exit temperature profiles determined both experimentally and computationally. This migration is caused by secondary flow development as the remnants of the passage vortices are still readily discernible at span locations of 0.1 and 0.9 percent in this wake region, as shown in the figure. Consequently, it is believed that these passage vortices, which develop from the vane leading edge horseshoe vortices, are more dominant within the passage.

The same increase in fluid temperature from the vane inlet to the vane exit is not seen near the OD endwall, but rather a reduc-

tion in temperature occurs for all four measured inlet profiles. Again, this is consistent with secondary flow migration toward the ID endwall. The differences in the measured exit temperature profiles with changing inlet profile are consistent with variations in the level of migration of OD flow toward the ID. Again, this is related to differences in the severity of the secondary flows. Since secondary flows are driven by radial and circumferential gradients in static pressure within the passage, it is instructive to consider the change in airfoil loading resulting from one profile versus another. Figure 13 is a plot of the static pressure on the vane normalized by the upstream total pressure (P_1). Both the pressure and suction surfaces are shown for both Inlet Profiles B and D. Clearly, it can be seen that the loading changes from ID to OD. This pressure variation has a profound effect on the radial and circumferential gradients in the velocity vectors within the passage. Again, this is consistent with the general conclusions of Munk and Prim [1]. Also note that the difference in static pressure between inlet Profiles B and D is significantly different near the OD driving even more flow down the vane span for inlet Profile D.

Conclusions

Several different radial profiles of pressure and temperature were analyzed at the inlet and exit of a fully annular high pressure turbine vane ring. The redistribution of the inlet profiles as the flow passed through the vane passages was examined and several important results were found. As the upstream total pressure is increased along the endwalls, there is an increase in total pressure loss across the vanes. The downstream pressure profiles taken within different vane pitch regions also tend to become more uniform in the pitch direction over the majority of the vane span. This result suggests that the secondary flow vortices are becoming stronger and are affecting a larger span and pitch region within the vane passage.

A temperature decrease was noticed near the OD and into the midspan region for each of the inlet profiles studied. As the total pressure near the OD endwall was increased, this temperature

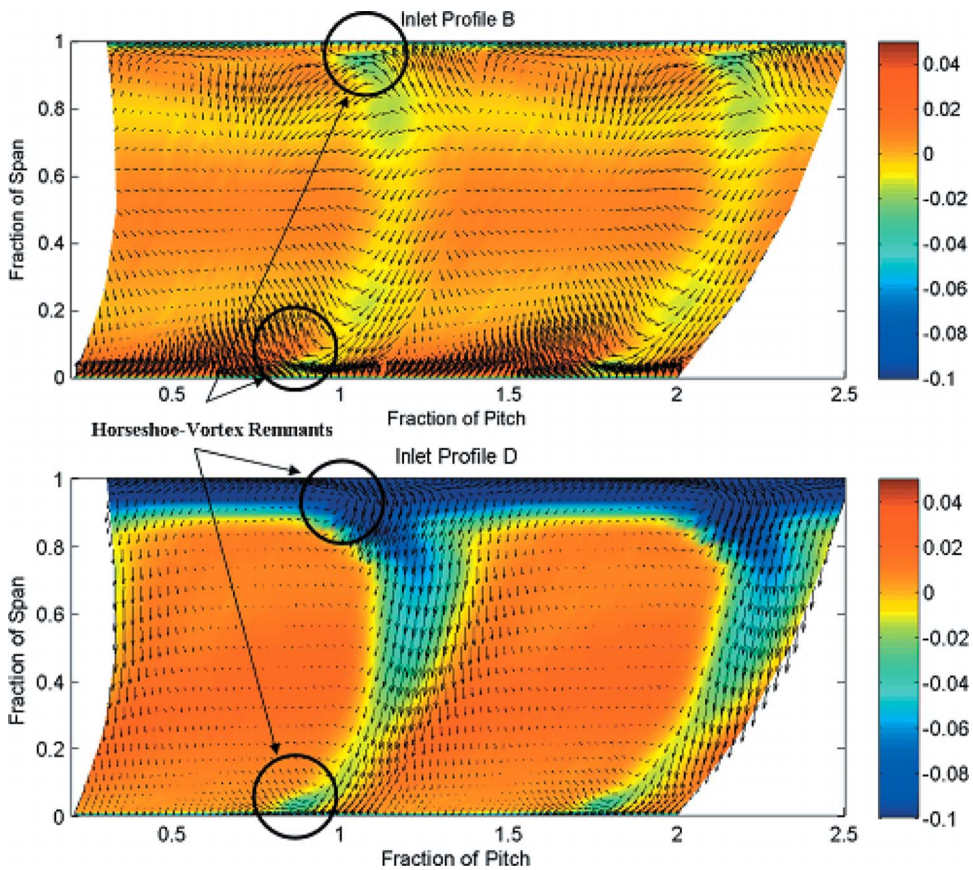


Fig. 12 Secondary flow vectors over contours of nondimensional exit temperature θ near the vane exit plane for Inlet Profiles B and D

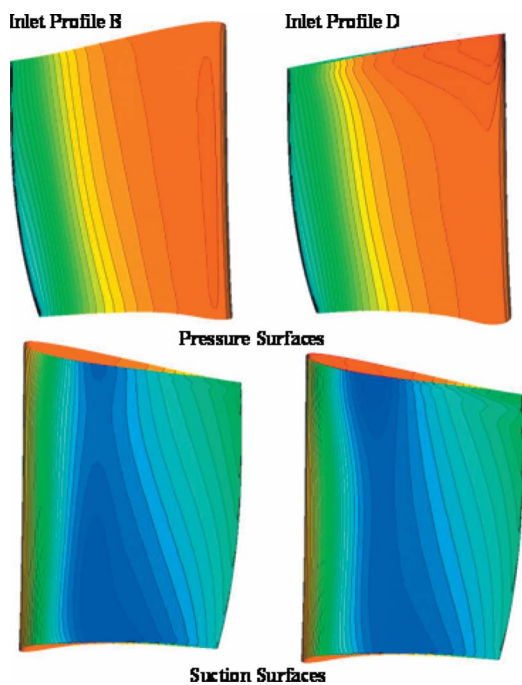


Fig. 13 Static pressure, normalized by P_1 , of the vane airfoil for Inlet Profiles B and D on the pressure surfaces and suction surfaces

reduction grew larger. This was caused by relatively cool fluid at a relatively high total pressure near the OD endwall being circulated toward the warmer and lower pressure midspan region. A temperature increase was observed near the ID for three of the four inlet profiles examined in this study. The one case in which there was no temperature increase was for a uniform inlet pressure field with uniform inlet temperature, and therefore no change in temperature was expected. For the other three cases, the increase in fluid temperature was attributed to the vane passage secondary flows directing the warmer core flow toward the ID endwall. The difference between the ID and OD exit temperature profile behavior is believed to be caused by the difference in the vane airfoil aerodynamic loading near the ID versus the OD. This spanwise difference in aerodynamic loading resulted in a different vane passage fluid migration and therefore changed the secondary flow circulation pattern.

Another important result from this study is that an increase in the total pressure along the endwalls at the vane inlet results in a decrease in the vane exit flow angle near the endwalls. This reduction in exit flow angle caused the flow to be oriented more in the axial direction. A relatively large pressure loss and change in exit flow angle were experienced near the OD for all of the inlet pressure profiles that were considered. This was attributed to large secondary flow vortices present within this span region. The exit flow angle results from this study are important when considering the design of a film cooling pattern located on the endwall platforms downstream of the vane. The results from this study are also important for considering the design of the downstream blade, which is heavily dependent on an accurate accounting of thermal conditions entering the airfoil row.

Acknowledgment

The authors would like to thank AFRL/PRTT and PRTE for their help in conducting these experiments as well as Robert Free for assembling the instrumentation rakes. The authors would also like to thank the Air Force Research Laboratory at Wright-Patterson Air Force Base for funding and sponsoring this research effort.

Nomenclature

- C = axial chord length of vane
 C_p = pressure coefficient,
 $C_p = (P - P_{MS_1}) / (1/2 \rho_{AVE} U_{AVE}^2 |_1)$
 P = total pressure, or vane pitch
 Re = Reynolds number, $Re = U_{ave} \cdot C / \nu_{ave}$
 S = vane span, or total vane surface length
 T = total temperature
TDC = top dead center of turbine vane ring
 Tu = turbulence intensity, $Tu = U_{rms} / U_{ave}$
 U = velocity
 X, Y, Z = axial, pitch, and span directions

Greek

- α = vane exit flow angle
 ϕ = circumferential location with respect to TDC
 ν = kinematic viscosity
 ρ = density
 θ = nondimensional temperature,
 $\theta = (T - T_{ave_1}) / (T_{ave_1})$
 ξ = percent total pressure loss, $\xi = 100 \cdot (P_1 - P_2) / P_1$
 $\bar{\xi}, \bar{\bar{\xi}}$ = mean and overall loss, $\bar{\xi} = \int_{\phi=0}^{\phi=P} \xi d\phi$,
 $\bar{\bar{\xi}} = \int_{r=OD}^{r=ID} \int_{\phi=0}^{\phi=P} \xi d\phi dr$

Subscripts

- 1 = upstream of vane
2 = downstream of vane
ave = mean, or average conditions across vane pitch
or span
ms = midspan

References

- [1] Munk, M., and Prim, R. C., 1947, "On the Multiplicity of Steady Gas Flows Having the Same Streamline Pattern," *Proc. Natl. Acad. Sci. U.S.A.*, **33**, pp. 137–141.
- [2] Langston, L. S., 1980, "Crossflows in a Turbine Cascade Passage," *ASME J. Eng. Power*, **102**, pp. 866–874.
- [3] Hermanson, K., and Thole, K. A., 1999, "Effect of Inlet Profiles on Endwall Secondary Flows," *J. Propul. Power*, **16**(2), pp. 286–296.
- [4] Colban, W., Thole, K., and Zess, G., 2002, "Combustor Turbine Interface Studies—Part 2: Flow and Thermal Field Measurements," ASME Paper No. 2002-GT-30527.
- [5] Boyle, R., and Giel, P., 1997, "Prediction of Nonuniform Inlet Temperature Effects on Vane and Rotor Heat Transfer," ASME Paper No. 97-GT-133.
- [6] Dorney, D., and Schwab, J., 1996, "Unsteady Numerical Simulations of Radial Temperature Profile Redistribution in a Single-Stage Turbine," *ASME J. Turbomach.*, **118**, pp. 783–791.
- [7] Cattafesta, L., 1988, "An Experimental Investigation of the Effects of Inlet Radial Temperature Profiles on the Aerodynamic Performance of a Transonic Turbine Stage," MS thesis, M.I.T., Cambridge.
- [8] Shang, T., Guenette, G., Epstein, A., and Saxer, A., 1995, "The Influence of Inlet Temperature Distortion on Rotor Heat Transfer in a Transonic Turbine," AIAA Paper No. 95-3042.
- [9] Chana, K., Hurrian, J., and Jones, T., 2003, "The Design, Development and Testing of a Non-Uniform Inlet Temperature Generator for the QinetiQ Transient Turbine Research Facility," ASME Paper No. 2003-GT-38469.
- [10] Povey, T., Chana, K., Jones, T., and Hurrian, J., 2005, "The Effect of Hot-Streaks on HP Vane Surface and Endwall Heat Transfer: An Experimental and Numerical Study," ASME Paper No. GT2005-69066.
- [11] Butler, T. L., Sharma, O. P., Joslyn, H. D., and Dring, R. P., 1989, "Redistribution of an Inlet Temperature Distortion in an Axial Flow Turbine Stage," *J. Propul. Power*, **5**(1), pp. 64–71.
- [12] Saxer, A., and Giles, M., 1990, "Inlet Radial Temperature Redistribution in a Transonic Turbine Stage," AIAA Paper No. 90-1543.
- [13] Barringer, M. D., Thole, K. A., and Polanka, M. D., 2009, "An Experimental Study of Combustor Exit Profile Shapes on Endwall Heat Transfer in High Pressure Turbine Vanes," *ASME J. Turbomach.*, **131**(2), p. 021009.
- [14] Haldeman, C. W., Dunn, M. G., MacArthur, C. D., and Murawski, C. G., 1992, "The USAF Advanced Turbine Aerothermal Research Rig (ATARR)," *NATO AGARD Propulsion and Energetics Panel Conference Proceedings*, Vol. 527, Antalya, Turkey.
- [15] Barringer, M. D., Thole, K. A., and Polanka, M. D., 2007, "Experimental Evaluation of an Inlet Profile Generator for High-Pressure Turbine Tests," *ASME J. Turbomach.*, **129**(2), pp. 382–393.
- [16] Dorney, D. J., and Davis, R. L., 1992, "Navier–Stokes Analysis of Turbine Blade Heat Transfer and Performance," *ASME J. Turbomach.*, **114**, pp. 795–806.
- [17] Rai, M. M., 1987, "Navier–Stokes Simulations of Rotor–Stator Interaction Using Patched and Overlaid Grids," *J. Propul. Power*, **3**, pp. 387–396.
- [18] Rai, M. M., and Madavan, N. K., 1990, "Multi-Airfoil Navier–Stokes Simulations of Turbine Rotor–Stator Interaction," *ASME J. Turbomach.*, **112**, pp. 377–384.
- [19] Prausner, T. J., Magowan, J. W., and Clark, J. P., 2003, "Predictions of Temperature Redistribution in a Turning Duct and in High-Pressure Turbines," ASME Paper No. GT2003-38317.
- [20] Clark, J. P., and Grover, E. A., 2006, "Assessing Convergence in Predictions of Periodic-Unsteady Flowfields," ASME Paper No. GT2006-90735.
- [21] Johnson, P. D., 2005, "Consortium Turbine Research Rig, Aerothermal and Mechanical Design," AFRL Technical Report No. AFRL-PR-WP-TR-2005-2157.
- [22] Urbassik, R. M., Wolff, J. M., and Polanka, M. D., 2006, "Unsteady Aerodynamics and Interactions Between a High Pressure Turbine Vane and Rotor," *ASME J. Turbomach.*, **128**, pp. 35–72.
- [23] Ames, F. E., Johnson, J. D., and Fiala, N. J., 2006, "The Influence of Aero-Derivative Combustor Turbulence and Reynolds Number on Vane Aerodynamic Losses, Secondary Flows, and Wake Growth," ASME Paper No. GT2006-90168.
- [24] Cumpsty, N. A., 1989, *Compressor Aerodynamics*, Longmans, New York, p. 316.